Journal Pre-proofs

UV/Fe^{II}NTA as a novel photoreductive system for the degradation of perfluorooctane sulfonate (PFOS) via a photoinduced intramolecular electron transfer mechanism

Zhuyu Sun, Chaojie Zhang, Jinchi Jiang, Jin Wen, Qi Zhou, Michael R. Hoffmann

PII: S1385-8947(21)02507-9
DOI: https://doi.org/10.1016/j.cej.2021.130923
Reference: CEJ 130923

To appear in: *Chemical Engineering Journal*

Received Date: 10 April 2021
Revised Date: 14 June 2021
Accepted Date: 16 June 2021

Please cite this article as: Z. Sun, C. Zhang, J. Jiang, J. Wen, Q. Zhou, M.R. Hoffmann, UV/Fe^{II}NTA as a novel photoreductive system for the degradation of perfluorooctane sulfonate (PFOS) via a photoinduced intramolecular electron transfer mechanism, *Chemical Engineering Journal* (2021), doi: https://doi.org/10.1016/j.cej.2021.130923

UV/Fe^{II}NTA as a novel photoreductive system for the degradation of perfluorooctane sulfonate (PFOS) via a photoinduced intramolecular electron transfer mechanism

Zhuyu Sun,[†‡] Chaojie Zhang,[*‡&] Jinchi Jiang,[&] Jin Wen,[¶£] Qi Zhou,[&] Michael R. Hoffmann[§]

[†]College of Environmental Science and Engineering, Donghua University, Shanghai, 201620, China

[‡]Shanghai Institute of Pollution Control and Ecological Security, Shanghai 200092, China

[&]State Key Laboratory of Pollution Control and Resources Reuse, College of Environmental Science and Engineering, Tongji University, Shanghai 200092, China

[¶]State Key Laboratory for Modification of Chemical Fibers and Polymer Materials & College of Materials Science and Engineering, Donghua University, Shanghai 201620, China

[£]Institute of Theoretical Chemistry, Faculty of Chemistry, University of Vienna, Währinger Str. 17, 1090 Vienna, Austria

[§]Linde-Robinson Laboratories, California Institute of Technology, Pasadena, California 91125, United States

*Corresponding author. Tel: +86 21 65981831; fax: +86 21 65983869;

E-mail address: myrazh@tongji.edu.cn

Abstract:

Perfluorooctane sulfonate (PFOS) is a persistent organic pollutant that is toxic and bio-accumulative. Previously, we used hydrated electrons (e_{aq}^-) generated by the UV photolysis of nitrilotriacetic acid (NTA) to initiate the photoreductive decomposition of PFOS. However, due to the protonation of NTA and the scavenging effect of H^+ on e_{aq}^-, this process relies highly on alkaline conditions. Herein, we report on an enhanced UV photoreductive system based on Fe^{II}NTA, which results in the decomposition of PFOS at pH 8.0 under anoxic conditions. After 10 hours of photolysis, the degradation and defluorination efficiencies of PFOS in the UV/Fe^{II}NTA system were ~60% and 29.5%, respectively, with a pseudo first-order degradation rate constant of k_{obs} = 0.081 h^{-1}. Laser flash photolysis results combined with time-dependent density functional theory (TDDFT) calculations indicate that PFOS, $Fe(H_2O)_6^{2+}$, and NTA form a penta-coordinated metal-ligand complex that undergoes a UV-induced directional electron transfer from Fe^{II}NTA to PFOS. PFOS decomposes via a mechanism that proceeds through a concerted photoinduced intramolecular charge transfer instead of direct attack by e_{aq}^-. Model chelate studies show that the inherent properties of the transition metal ion and the electron-donating capabilities of the complexing ligands determine the efficiency for photoreductive electron transfer. A low apparent activation energy of 4.74 kJ/mol over a broad pH range results in higher electron transfer efficiencies for UV/Fe^{II}NTA photolysis compared to photolysis initiated by un-complexed NTA.

Keywords: Perfluorooctane sulfonate (PFOS); Photocatalysis; Reductive defluorination; Intramolecular electron transfer

1. Introduction

Per- and polyfluoroalkyl substances (PFASs, C_nF_{2n+1}−R) refer to a family of anthropogenic chemicals that most often contain a hydrophobic perfluoroalkyl chain and a hydrophilic functional end group. Due to their unique physico-chemical properties, PFASs have been extensively produced and utilized in various industrial and commercial applications since the 1940s [1, 2]. More than 3000 PFASs are presently or previously on the global chemical market [3, 4]. The PFAS family of compounds show strong persistence, high bioaccumulation and toxicity, and pose long-term risks to the environment, biota and humans [5, 6]. Perfluorooctane sulfonate (PFOS, $C_8F_{17}SO_3^-$) is the first representative PFASs that was added to the Stockholm Convention on Persistent Organic Pollutants (POPs) in 2009. Due to the excellent physicochemical properties, such as the strong thermal and chemical stability, high surface activity, and the water- and oil-repellency, PFOS has been used in a wide variety of industrial and consumer applications (e.g. metal plating and cleaning, textile treatment, fire-fighting foams, semiconductor industry, and surface protectors in carpets, leather, paper, packaging, fabric, and upholstery) [2, 4]. **Paul et al.** estimated that ~ 45250 t PFOS was released to the environment between 1970−2012 from direct (manufacture, use, and consumer products) and indirect (PFOS precursors and/or impurities) sources [7]. However, in the past decade, increasing toxicological researches have shown that PFOS is related to epigenetic changes, developmental toxicity, immunotoxicity, hepatotoxicity, and endocrine disruption [5, 8, 9]. Additionally, because of the high bonding energy of C-F bond (485 kJ/mol) and strong

electronegativity of fluorine (4.0), PFOS is extremely resistant to hydrolysis, pyrolysis, photolysis and biological degradation, which makes it highly persistent in the environment [2].With an oxidation potential higher than +2.0 V (*vs.* NHE) and a reduction potential lower than -1.3 V [10], PFOS is difficult to be effectively decomposed by conventional water treatment technologies [11, 12].

At present, advanced treatment technologies, such as photocatalysis [13], sonochemical degradation [14], zerovalent iron reduction in subcritical water [15], nanoscale bimetallic catalytic reduction [16], microwave decomposition [17], electrochemical treatment [18] and plasma chemical degradation [19], have been explored for PFOS decomposition. Among these alternatives, photoreduction via hydrated electron (e_{aq}^-) production is attractive due to the reactivity and nucleophilicity of e_{aq}^- (E= –2.9 V), toward halogenated organic contaminants [20]. In a previous study, we reported on a photoreductive system for PFOS degradation using e_{aq}^- released from photoactivated nitrilotriacetic acid (NTA), which was used as a benign sacrificial electron donor [21]. However, speciation of NTA depends on pH (i.e. pK_{a1} = 1.89, pK_{a2} = 2.49, pK_{a3} = 9.73) and complete deprotonation is critical for the effective generation of e_{aq}^-. As a consequence, the efficiency of UV/NTA photolysis depends greatly on pH (e.g. pH > 9.7), which may limit its potential engineering application [21]. In fact most photolytic systems generating e_{aq}^- (e.g. UV/KI [22], UV/sulfite [23], UV/p-benzoquinone [24], etc. [25]), require strong alkaline conditions to prevent the rapid consumption of e_{aq}^- by protons. In addition, due to the low absorption coefficient of NTA at 254 nm, the transient yield of e_{aq}^- by UV/NTA process is low [21]. Therefore,

developing new approaches that can achieve effective degradation and defluorination of PFOS under circumneutral conditions is desirable.

For the past decades, transition-metal-catalyzed reaction has become a rapidly growing area of research due to the excellent properties of transition-metal ions in reversible ligation, electron transfer, light-harvesting, catalytic transformation and opening new reaction pathways [26-29]. Previous studies show that a dynamic Fe^{2+}/Fe^{3+} redox cycle can enhance the photodecomposition of PFOS and PFOA under UV [30-32] and VUV [33, 34] illumination. However, $Fe(H_2O)_6^{2+}$ and $Fe(H_2O)_6^{3+}$ are only stable in very acidic conditions (pH<4). Under neutral or alkaline conditions, Fe^{2+} and Fe^{3+} ions are easy to precipitate in the form of oxyhydroxide iron species [35]. Thus, under normal condition in the absence of chelation, the catalytic effects of Fe^{2+}/Fe^{3+} is only applicable at low pH [33, 36, 37]. Complexation of Fe^{II} and Fe^{III} with aminopolycarboxylic acids (APCAs) and carboxylates can extend the pH range for redox catalysis [38]. For example, NTA forms stable complexes with Fe^{2+} and Fe^{3+} [39, 40]. Since Fe^{II}NTA and Fe^{III}NTA complexes are soluble over a wide pH range of 2-10 [39], they can be potentially used as photocatalysts or photolytic sources of e_{aq}^- under UV 254 illumination at circumneutral pH. Furthermore, depending on the specific chelating agents the oxidation-reduction potentials and photon absorption capacities of the metal-ligand complexes can be shifted [41]. The apparent catalytic effects of Fe^{II}NTA and Fe^{III}NTA redox have been explored for enhancing photo-Fenton oxidation [39], persulfate activation [42], cytochrome c reduction [43] and electro-Fenton reactions [44]. Moreover, the 2nd-order rate constant of Fe^{II}NTA with •OH at

circumneutral pH (5.0×10^9 $M^{-1}\cdot s^{-1}$, pH=6.2) [45] is higher than Fe^{2+} + •OH (3.5×10^8 $M^{-1}\cdot s^{-1}$, pH=4.5-6.2) [20] and NTA + •OH (5.5×10^8 $M^{-1}\cdot s^{-1}$, pH=6.0) [46], therefore Fe^{II}NTA may have a higher efficiency in preventing the geminate recombination of e_{aq}^- with •OH.

Given the enhanced photocatalytic potential of the Fe(II/III)-ligand complexes, we now explore the efficiency of UV/Fe-NTA system on the degradation and defluorination of PFOS. The novel photolytic system aims to realize efficient degradation and defluorination of PFOS under relatively mild conditions with eco-friendly additives. Herein, we also report on the possible catalytic mechanism based on laser flash photolysis experiment, UV-Vis characterization, TDDFT calculations and on the variation of model chelating agents. The parametric effects of temperature, pH, Fe^{II}/NTA molar ratios and actual Fe^{II}NTA concentrations are also reported.

2. Materials and Methods

2.1. Chemicals

Perfluorooctanesulfonic acid (PFOS, ~40% in water), nitrilotriacetic acid trisodium salt (NTA, ≥98.0%), trisodium citrate (CA, ≥99.0%), HPLC grade ammonium acetate (99.99%) and methanol (≥99.99%) were purchased from Sigma-Aldrich Chemical Co. (St. Louis, Mo, USA). Ferrous sulfate heptahydrate (≥99.0%), ferric sulfate pentahydrate (≥97.0%), cobalt(II) sulfate heptahydrate (≥99.5%), copper(II) sulfate pentahydrate (≥99.0%), diethylenetriaminepentaacetic acid pentasodium salt (DTPA, ≥99.0%), iminodiacetic acid (IDA, ≥98.0%), methylglycine diacetic acid trisodium salt (MGDA, ≥99.0%), ammonium hydroxide solution (25%),

ammonium chloride (≥99.8%), sodium hydroxide (≥96.0%) and hydrochloric acid (36.0%-38.0%) were obtained from Sinopharm Chemical Reagent Co. (Shanghai, China). Sodium perfluoro-1-[1,2,3,4-$^{13}C_4$]octanesulfonate (MPFOS, ≥99%, $^{13}C_4$) used as the internal standard for the quantification of PFOS was acquired from Wellington Laboratories Inc. (Guelph, ON, Canada). Milli-Q water and deionized water were used throughout the whole experiment.

2.2. Reductive defluorination

The photoreductive degradation of PFOS was conducted under anoxic conditions in a stainless steel cylindrical reactor as reported previously [21] (**Fig. S1, SI**). The outer and inner diameters of the reactor were 100 mm and 60 mm, respectively. A low-pressure mercury lamp (14 W, Heraeus, Germany) with quartz tube protection was placed in the center of the reactor, emitting 254 nm UV light. The incident photon intensity in this system was determined to be 2.17×10^{-6} Einstein L^{-1} s^{-1} by iodide/iodate actinometry using the intrinsic quantum yield of 0.81 for iodide/iodate as a reference [47]. Solutions of Fe^{II}NTA were synthesized in a N_2 atmosphere by mixing $FeSO_4$ (0.3 mM) and NTA (2 mM) in deoxygenated water for 30 mins. All Fe^{II}NTA solutions were freshly prepared each time before use. Then 720 mL solution containing PFOS (0.01 mM) and Fe^{II}NTA was added to the reactor. Before the reaction, the mixture was bubbled with highly purified nitrogen for 30 mins. The initial solution pH was adjusted to desired values with 0.1 M HCl or NaOH. The study was carried out in the absence of acetate, phosphate or ammonium buffer to preclude any complexation with Fe ions. The reaction temperature was held constant at 30 °C by a circulating cooling system.

After various time intervals, samples of the liquid were analyzed after filtration through 0.22 μm nylon filter (ANPEL Laboratory Technologies, Shanghai, China) or centrifugation.

2.3. Analytical methods

The concentrations of PFOS versus time were determined by high-performance liquid chromatography/tandem mass spectrometry (HPLC−MS/MS, TSQ™ Quantum Access™, Thermo Finnigan, San Jose, CA, USA). The formation of fluoride was quantified by ion chromatography equipped with a conductivity detector (Dionex, ICS-3000, Thermo Fisher Scientific, USA). More detailed information is available in the **SI**.

2.4. Laser flash photolysis experiment and UV-Vis characterization

Nanosecond laser flash photolysis for the detection of e_{aq}^- was performed using an LP980 Edinburgh instrument (UK) with laser excitation at 266 nm from a Surelite I-10 Q-Switched Nd:YAG laser (35 mJ). Components of the laser flash photolysis apparatus were as described by **Jin et al.** [48]. Detailed information about the instrument and experiment is available in the **SI**.

The UV-Vis spectra were recorded at room temperature with a Shimadzu spectrophotometer (UV-1900i, Shimadzu, Japan). Samples containing Fe^{II}NTA were prepared in a glovebox (Super 1220/750/900, Mikrouna Co. Ltd., Shanghai, China) with deoxygenated Milli-Q water.

2.5. DFT calculations

The geometrical optimization was carried out at the B3LYP [49, 50]/6-31G(d) [51-56] level with Grimme's D3BJ empirical dispersion-corrected density fuctional theory

(DFT) [57] using Gaussian16, Revision B.01 [58]. The time-dependent density fuctional theory (TDDFT) calculations were performed at the CAM-B3LYP[59]/6-311G(d)[60] level with Grimme's D3 dispersion correction [61] to simulate the absorption spectra. Three different functionals, CAM-B3LYP, B3LYP and M062X [62] were compared with the experimental spectra to further analyze the electronic structure in the excited state. The CAM-B3LYP functional gave the best agreement with the measured spectra. The first 70 TDDFT excited states were simulated based on the optimized structure in the ground state. The hole-electron distribution was analyzed using Multiwfn [63] and the figures were rendered with VMD [64].

2.6. Calculations

The PFOS degradation and defluorination ratios were calculated as follows:

$$\text{Degradation ratio} = \frac{[\text{PFOS}]_0 - [\text{PFOS}]_t}{[\text{PFOS}]_0} \times 100\% \quad (9)$$

$$\text{Defluorination ratio} = \frac{[F^-]_t}{[\text{PFOS}]_0 \times 17} \times 100\% \quad (10)$$

where $[\text{PFOS}]_0$ and $[\text{PFOS}]_t$ are the PFOS concentrations at the start of the reaction and at the irradiation time t, respectively. $[F^-]_t$ refers to the concentration of fluoride ions at time t.

3. Results and Discussion

3.1. Photodegradation and defluorination of PFOS by UV/Fe^{II}NTA system

The λ = 254 nm photochemical decomposition of PFOS was carried out at pH 8.0 under anoxic conditions. In order to determine the synergistic effect of Fe^{II} and NTA, three control experiments were conducted. The results are shown in **Fig. 1**. Since PFOS has no appreciable absorption at 254 nm [65], the direct photolysis of PFOS (the 3rd control experiment) was shown to be negligible. The 10-h degradation and defluorination ratios of PFOS were only 4.7% and 0.9%, respectively. Adding 0.3 mM Fe^{2+} (the 2nd control experiment) didn't result in obvious increases in PFOS degradation and defluorination, which seems contradictory to the results of previous studies that Fe^{2+}/Fe^{3+} cycle can effectively catalyze the photodecomposition of PFOS [30]. The inefficiency of Fe^{2+} in this study can be ascribed to three aspects. 1) Fe^{2+}/Fe^{3+} is only stable in strong acidic condition [35], while at pH above 4-5 the catalytic reaction cannot proceed because of formation of inactive and insoluble iron precipitation. 2) The actual active Fe ion that can catalyze PFOS decomposition is Fe^{3+} and the complexation between Fe^{3+} and PFOS is a prerequisite [66]. The Fe^{III}-PFOS complex undergoes photooxidation via a ligand-to-metal charge transfer (LMCT) process [30]. However, Fe^{2+}, which cannot directly catalyze the photooxidation of PFOS, was used in this study. 3) Decomposition of the transient PFOS radical after a LMCT requires the involvement of O_2 and •OH [30], which were not present under the anoxic conditions. The recovery of Fe^{3+} from Fe^{2+} also requires O_2 for a continuous catalysis of PFOS degradation [67]. Therefore, Fe^{2+} cannot mediate the photodecomposition of PFOS under the

aforementioned conditions.

Addition of 2 mM NTA (1st control experiment) significantly accelerated the photodegradation of PFOS. The 10-h degradation and defluorination ratios of PFOS were 43.3% and 14.9%, respectively. The mechanism of UV/NTA system has been elucidated in our previous study [21]. However, compared with the strong alkaline condition, PFOS degradation and defluorination were significantly suppressed at pH 8.0. For instance, the 10-h degradation and defluorination ratios of PFOS at pH 8.0 in this study were 2.0-fold and 3.1-fold, respectively, lower than those obtained at pH 10.0 [21]. Therefore, the high efficiency of the UV/NTA photolytic system for degrading PFOS is limited by the requirement for high pH in potential scaled-up engineering applications.

Adding 0.3 mM Fe^{2+} to 2 mM NTA to form Fe^{II}NTA complex (the treatment experiment) enhanced the decomposition and degradation of PFOS at pH 8.0. The 10-h PFOS degradation and defluorination ratios increased to 59.9% and 29.5%, respectively. PFOS degradation in the UV/Fe^{II}NTA system follows pseudo-first-order kinetics (**Fig. S3, SI**), with an observed rate constant k_{obs} = 0.081 h^{-1}, and a corresponding half-life time $t_{1/2}$ = 8.6 h. The observed rate constant for PFOS decomposition in the UV/NTA system at pH 8.0 was only 0.055 h^{-1} ($t_{1/2}$ = 12.6 h). The k, $t_{1/2}$ values and energy consumption of some other treatments such as direct UV, UV/persulfate, UV/Fenton(Fe^{3+}), sonolysis and electrolysis, are summarized in **Table S1** in the **SI**. Overall, UV/Fe^{II}NTA system has a satisfactory performance and a moderate energy consumption of 120.4 kJ/μmol. Even though the UV/Fe^{II}NTA process

has a lower PFOS degradation rate constant than UV/KI (0.18 h^{-1}) and UV/sulfite (0.16 h^{-1}), it still has potential applications under circumneutral conditions, and causes relatively low secondary pollution risks.

3.2. Mechanism of the photodegradation of PFOS by UV/Fe^{II}NTA system

The photochemical experimental results indicate that UV/Fe^{II}NTA system has a good performance in PFOS degradation and defluorination under the weakly alkaline conditions (pH 8.0). According to the results of **Jin et al.**, Fe^{3+} can mediate the decomposition of PFOS via a photocatalytic oxidation mechanism of LMCT [30]. Therefore, determination of the actual Fe speciation is critical to understand Fe-ligand photo-redox processes. The aqueous Fe^{II} and Fe(total) concentrations were determined with a UNICO spectrophotometer (UV-2800, UNICO, USA) based on the 1,10-phenanthroline method [68]. According to the results in **Table. S2**, **SI**, the majority of Fe (> 92%) was present as Fe^{2+} during the reaction process, suggesting that Fe^{2+} is the active species, which implies that PFOS undergoes decomposition via a potential photo-reductive pathway.

Our previous study demonstrated that e_{aq}^- plays a key role in the photoreductive decomposition of PFOS in UV/NTA system [21]. Furthermore, it has previously been shown that Fe ions could induce a redox reaction between Fe-NTA and a water as a ligand at λ = 254 nm, resulting in water dissociation and generation of radicals [69]. Therefore, we conducted a laser flash photolysis study to characterize e_{aq}^-. The results are shown in **Fig. 2**. The transient absorption spectra of intermediates were obtained at 10 nm intervals between 300 nm and 750 nm upon the photolysis of Fe^{II}NTA in N_2

saturated water (**Fig. 2a**). The broad optical absorption band with a peak at around 700 nm is attributed to e_{aq}^- according to previous theoretical [70] and experimental [71] characterizations. However, the absorption peak of e_{aq}^- decayed quickly within 0.3-0.4 μs, indicating that e_{aq}^- was rapidly quenched. The decays of e_{aq}^- in the presence of PFOS with different concentrations are shown in **Fig. 2b**. Adding PFOS accelerated the decay of e_{aq}^-, and the decay rate increased with an increase in PFOS concentration. However, compared with the UV/NTA system, the impact of PFOS on e_{aq}^- decay in UV/Fe^{II}NTA system was much smaller. For instance, the half-life of e_{aq}^- in UV/Fe^{II}NTA system decreased by 1.39-fold and 1.52-fold, respectively, with the addition of 50 μM and 500 μM PFOS, whereas in UV/NTA system, it decreased by 1.84-fold and 2.9-fold, respectively, with the addition of 10 μM and 100 μM PFOS. This result implies that e_{aq}^- may not be the only viable pathway responsible for PFOS decomposition in UV/Fe^{II}NTA system. This conclusion can be further supported by the e_{aq}^- yield comparison under different conditions (**Fig. 2c and 2d**). In the UV/NTA system at pH 10.0, the transient yield of e_{aq}^- was much higher with a longer half-life, which makes UV/NTA system have a good performance under strong alkaline conditions [21]. However, at pH 8.0, the transient yield and the half-life of e_{aq}^- both decreased dramatically (**Fig. 2c)** due to the protonation of NTA and the scavenging effect of H^+. Therefore, UV/NTA system has a low efficiency under circumneutral conditions. However, compared with the UV/NTA system at pH 8.0, the generation of e_{aq}^- in UV/Fe^{II}NTA system was even weaker (reflected by the half-life of e_{aq}^-, which was only 0.18 μs in UV/Fe^{II}NTA system in contrast to the 2.14 μs in UV/NTA system). Therefore,

even though these two systems have comparable transient yields of e_{aq}^- at pH 8.0, their steady-state concentrations of e_{aq}^- differ a lot. These results mean that the photoinduced generation of e_{aq}^- from NTA was greatly inhibited by the coordinated transition metal. A plausible explanation is that the generated e_{aq}^- are easily trapped by the empty d orbitals of Fe^{III}, thus leading to an efficient back reaction and a short half-life of e_{aq}^-. Anyhow the weak generation and short half-life of e_{aq}^- cannot explain the improved performance of UV/Fe^{II}NTA system compared to the UV/NTA system (**Fig. 1)**, suggesting that e_{aq}^- is not the primary pathway for PFOS decomposition in the UV/Fe^{II}NTA system. Other mechanisms should be taken into consideration. Furthermore, in order to gain insight, other metal-NTA complexes including Co^{II}NTA, Cu^{II}NTA and Fe^{III}NTA were investigated for the photoinduced generation of e_{aq}^-. These results are discussed in **section 3.3**.

NTA is an APCA which contains three carboxylate groups bound to a nitrogen atom. APCAs have strong chelating effects with first-row transition metal ions. For instance, Fe-APCA complexes are commonly found in aqueous solution as monomeric or dimeric species, with the monomeric one dominant (>80%) [39]. Multi-dentate metal-ligand complexes can enhance the UV-Vis absorption of APCAs and extend their absorption spectra to longer wavelengths (**Fig. S4a, SI**). For instance, the absorbance of 10 mM NTA (pH 8.0) at λ = 254 nm is only 0.031, whereas the value increases to 0.398 when complexed with 1.5 mM Fe^{2+}. Therefore, metal-NTA complexation can significantly enhance the photon adsorption, which should increase the quantum yield of the overall photochemical process. Moreover, Fe^{2+} and Fe^{3+} are both octahedral

coordinated, while NTA is a tetradentate ligand. So the coordination around Fe^{2+}/Fe^{3+} is completed by two water molecules to form the Fe^{II}NTA or Fe^{III}NTA complex (**Fig. S5, SI**) [69]. In the pH range of 2-10, equilibrium exist among the protonated form, the monohydroxy anion, and the dihydroxy anion as shown in **Fig. S5, SI** [39]. However, when PFOS is present in the solution, the sulfonate group of PFOS has the potential to substitute for water or hydroxide in coordination spheres of Fe^{2+}/Fe^{3+}. Complexation of PFOS is actually detected in the UV-Vis spectra as illustrated in **Fig. S4b, SI**. When PFOS is added to the aqueous solution of Fe^{II}NTA, the UV absorbances over the wavelength range of 240-330 nm increased obviously. A shoulder at ~260 nm is consistent with a change in the coordination environment of Fe^{II} due to ligand substitution by PFOS. Moreover, the absorption increases also suggest an enhanced photodetachment of the complex under 254 nm irradiation.

Therefore, in order to further confirm the coordination geometry of the [PFOS, OH^- and Fe^{II}NTA] complex and to investigate its photoexcitation under 254 nm irradiation, a density functional theory (DFT) calculation was carried out. The geometrically optimized structure of the [PFOS, Fe^{II}, NTA] complex is shown in **Fig. S6** in the **SI**. According to the calculated ΔG^o, the pentacoordinated Fe^{II} complex with the ligands PFOS and NTA is more stable compared to the hexacoordinated Fe^{II} complex with PFOS, OH^- and NTA as ligands. Furthermore, the sulfonate group serves a monodentate ligand on Fe^{II} due to geometric limitations; bidentate coordination of the sulfonate group is prevented. Based on the pentacoordinated geometry of the [PFOS-Fe^{II}-NTA] complex, a TDDFT calculation was further carried out to characterize the

photoexcitation, photoionization and charge transfer processes. As is shown in **Fig. S7, SI**, the simulated spectrum closely matches the experimental spectrum (**Fig. S4b, SI)**. Both have an intense band at 200 nm and a shoulder at ~260 nm. A total of 70 excited states and their corresponding electronic transitions were computed. The computed spectrum contains three adjacent excited states >254 nm (257.80 nm, 279.34 nm and 322.20 nm), corresponding to the excitations involving the MOs in the range of α-HOMO to α-LUMO and β-HOMO to β-LUMO+1 (**Fig. 3**). These excited states along with the other two around 254 nm (243.5 nm and 248.9 nm) were summarized in **Table S3, SI**. The relevant MOs are shown in **Fig. S8** in the **SI**. The nature of these excitations are interpreted on the basis of the orbital composition of the frontier MOs. In general, the HOMOs (α and β) of the complex are located in Fe^{II} and NTA, and the LUMOs (α and β) are located in the antibonding orbitals in the PFOS region. This observation implies that all the above-mentioned excitations correspond to charge transfer from Fe^{II}NTA to PFOS. For instance, the excited state at 257.80 nm originates primarily from α-HOMO(185)→α-LUMO(186) (percentage contribution of 94.5%), which shows a significant Fe^{II}NTA→PFOS charge transfer character. Likewise, the β-HOMO(181)→β-LUMO(182)/β-LUMO+1(183) transfers are consistent with a Fe^{II}→PFOS MLCT. These excited states, especially the 257.8 nm, may play important roles in the photochemistry of UV 254 nm system. **Gu et al.** [23] suggested that after the electron was transferred to PFOS, it would prefer to localize in the molecular region covering the C4, C5, C6, C7 and C8 positions of PFOS ($C_8F_{17}SO_3^{\bullet 2-}$). This consequent delocalization would provide a sufficient force to weaken C-C and C-F sigma bonds,

which should result in PFOS dissociation. In addition to the frontier MOs, the hole-electron distributions of three excited states (at 257.80 nm, 248.90 nm and 243.71 nm) are illustrated in **Fig. S9, SI**; they are also consistent with the frontier MOs analysis of electron transfer to PFOS with a hole vacancy remaining in the Fe^{II}NTA region after photoexcitation.

Based on the results of the laser flash photolysis study, UV-Vis spectral characterizations and the TDDFT calculations, it is concluded that PFOS decomposition in UV/Fe^{II}NTA system occurs via a photoinduced intramolecular charge transfer mechanism instead of proceeding via direct ejection of e_{aq}^-. PFOS, Fe^{II} and NTA initially form a pentacoordinated complex, which allows for a photoexcited intramolecular electron transfer from the Fe^{II}NTA moiety to PFOS (**Eq. 1**). Then PFOS undergoes reductive degradation along with the oxidation of Fe^{II}NTA to form either Fe^{III}NTA or NTA oxidation products.

$$\mathrm{PFOS} + \mathrm{Fe}^{2+} + \mathrm{NTA} \rightarrow \left[\mathrm{PFOS} - \mathrm{Fe}^{\mathrm{II}} - \mathrm{NTA}\right] \mathrm{complex} \xrightarrow{\mathrm{hv}} \mathrm{PFOS\ degradation} \quad (1)$$

3.3. Metal ligand effects

In order to test the effect of other transition metal ions and multidentate chelating ligands, and to further explore the pathways and their activities, Co^{2+}, Cu^{2+} and Fe^{3+} complexed with NTA, and Fe^{2+} complexed with DTPA, IDA, CA and MGDA were chosen to investigate structure-activity relationship of the model chelates in the mediation of the photodegradation of PFOS. The structural formulas of the ligands are shown in **Table S4**, **SI**. The results of the model chelate study are shown in **Fig. 4**.

As can be seen in **Fig. 4A**, the transition metal ions show different effects in

mediating the photodegradation and defluorination of PFOS. Compared with the UV/NTA system, Fe^{II}NTA and Fe^{III}NTA show obvious enhancement effects, whereas Co^{II}NTA and Cu^{II}NTA have inhibitory effects. The overall comparable efficiencies of Fe^{II}NTA and Fe^{III}NTA can be attributed to the Fe^{II}/Fe^{III} redox cycle under UV irradiation. As discussed in **section 3.2**, Fe^{II} is considered as the dominant active form in mediating the photodecomposition of PFOS. After the photoexcited charge transfer, Fe^{II} was converted to Fe^{III}, which can be rapidly reduced to Fe^{II} in the presence of NTA under 254 nm irradiation [69]. Furthermore, along with Fe^{II}, NTA contributes to the HOMOs of the [PFOS-Fe^{II}-NTA] complex (**Fig. S10, SI**). Therefore, Fe^{III} is also able to achieve a high efficiency in the presence of reductive ligands. The slightly higher efficiency of Fe^{III} than Fe^{II} in the initial phase may be ascribed to the stronger photon absorption of Fe^{III}NTA than Fe^{II}NTA at λ 254 nm (**Fig. S4a, SI**). Co^{II} slightly inhibited the effect of NTA, while the inhibitory effect of Cu^{II} was much clearer. These results were derived from the apparent negative effects of Cu^{II} and Co^{II} on the generation of e_{aq}^- (**Fig. 2d**). The transient yield and half-life of e_{aq}^- in UV/Co^{II}NTA system were much lower than in the UV/NTA system, while no discernable signal of e_{aq}^- was observed in UV/Cu^{II}NTA system. Therefore, the decomposition of PFOS was partially suppressed due to the inefficient generation of e_{aq}^-. On the other hand, although the effect of e_{aq}^- was minimized, Co^{II}NTA and Cu^{II}NTA may play a role in the intramolecular electron transfer process, especially in light of the strong photon absorption for Cu^{II}NTA(**Fig. S4a, SI**). However, the catalytic efficiencies of Co^{II} and Cu^{II} were much lower than that of Fe^{II} and Fe^{III}, which was possibly derived from the

nature of the transition metal ions. **Hori et al.** indicated that the activity of metals in enhancing PFOS decomposition in subcritical water follows an increasing order of no metal ≈ Al < Cu < Zn << Fe [15]. **Bao et al.** reported that Fe is most effective for C-F bond activation by forming an PFSAs-metal-H intermediates that resulted in a lowered potential energy surface of the corresponding transition state [72].

In addition to the transition metal ions, the effects of the different ligands were also tested (**Fig. 4**). In general, except for MGDA, complexation of chelating ligands with Fe^{II} improves the photoreaction efficiency. The relative enhancements in reactivity followed the order of DTPA > NTA > IDA > CA. This order may be due to the number of the electron donating groups in the ligands. As was previously discussed, the acetate and amine groups play important roles in UV/APCAs systems [21]. Similarly, the coordinated carboxylate groups and the amine group (N) contribute to the occupied MOs (αHOMO-2−αHOMO and βHOMO-2−βHOMO) of the [PFOS-Fe^{II}-NTA] complex (**Fig. S10, SI**). Therefore, with more binding sites, DTPA and NTA have a greater MLLCT (Fe^{II}APCAs→PFOS) capacity and resultant efficiency. However, MGDA showed a converse pattern compared to the other chelators in that MGDA had a higher efficiency than Fe^{II}MGDA complex in mediating the degradation and defluorination of PFOS. This phenomenon is due to the fact that the electron-donating effects of methyl group attached to the α-carbon of the amine in the MGDA molecule enhances the UV generation of e_{aq}^-; therefore, the UV/MGDA system already has a relatively high efficiency. Furthermore, the methyl group impacts the complexation of MGDA with Fe^{II}, which is illustrated by the lower stability constant for Fe^{II}MGDA.

The metal-ligand bond strength may also influence the electron transfer process [43]. Thus, complexation of MGDA with Fe^{II} did not enhance the observed efficiency of MGDA.

The actual effect of a specific metal-ligand complex depends on the nature of the metal ions and the structure of the ligands. In some cases, complexation with metal ions decreases the relative photoreaction efficiency of the ligands. Complexes of Fe^{II}/Fe^{III} with the various APCAs with more donor moieties have higher efficiencies. The catalytic character of Fe and the improved MLLCT efficiency may play a crucial role.

3.4. Influential experimental parameters

3.4.1 Temperature

The effect of temperature on the photodegradation and defluorination of PFOS in the UV/Fe^{II}NTA system is shown in **Fig. S11** in the **SI**. Raising the temperature from 30 °C to 50 °C slightly increases the degradation rate and defluorination extent of PFOS. The 10-h degradation ratios of PFOS at the temperature of 30 °C, 40 °C, 50 °C were 59.9%, 60.3% and 63.2%, respectively; the 10-h defluorination ratios of PFOS were 29.5%, 29.5% and 31.1%, respectively. The pseudo first-order rate constants at the different temperatures showed little variation (i.e. 0.081 h^{-1}, 0.086 h^{-1} and 0.091 h^{-1}, respectively, at 30 °C, 40 °C and 50 °C). The apparent activation energy was determined from an Arrhenius plot as shown in **Fig. S11d, SI**. Based on the temperature dependence of the measured rate constants, the overall apparent activation energy (E_a) was calculated to be 4.74 kJ/mol. The E_a value is much lower than those obtained in the photoreductive decomposition of PFOA in UV/KI system (59.54 kJ/mol) [73] and in

the PFOA pyrolysis (154±11 kJ/mol) [74]. The observed E_a is lower than the activation energies of the e_{aq}^- reactions, which lie in the range of 6-30 kJ/mol [20]. **Buxton et al.** indicated that diffusion controlled reactions of most solutes in water have activation energies between 10 to 18 kJ/mol [20]. These results further confirm that PFOS degradation in the UV/Fe^{II}NTA system may occur via intramolecular electron transfer, which saves the energy for electron solvation and its subsequent diffusion to the substrate.

3.4.2 pH

According to previous studies, pH is an important variable that impacts PFOS degradation. In the case of UV/NTA photolysis under acidic conditions, e_{aq}^- is readily quenched by reaction with H^+, and the increased extent of NTA protonation results in a decrease in the yield of e_{aq}^- [21]. Therefore, efficient degradation and defluorination of PFOS in UV/NTA system occurs preferably at high pH. In contrast, as shown in **Fig. S12A, SI**, the highest efficiency observed in UV/Fe^{II}NTA system was obtained at pH 8.0. For instance, as the initial solution pH increased from 5.0 to 8.0, the 10-h degradation ratio of PFOS increased from 34.0% to 59.9%; the 10-h defluorination ratio of PFOS increased from 17.0% to 29.5%. However, as pH increases from 8.0 to 10.0, a decrease in 10-h PFOS degradation ratio (from 59.9% to 48.0%) and a decrease in 10-h PFOS defluorination ratio (from 29.5% to 25.8%) are observed. This effect can be attributed to the increasing [OH^-] that leads to substitution of carboxylate ligand by hydroxide on the Fe^{II}NTA complex with the subsequent precipitation of Fe^{II} as $Fe^{II}(OH)_2$ (K_{sp} = 8×10^{-16}) [42]. Therefore, different from the UV/NTA system, very

alkaline conditions on the contrary reduce the degradation and defluorination efficiencies of PFOS in UV/Fe^{II}NTA system. The optimum pH for UV/Fe^{II}NTA process was 8.0. Furthermore, the impact of pH for UV/Fe^{II}NTA system is not as significant as in the UV/NTA system. Weak acidic conditions (pH of 5.0 and 6.0) have moderate efficiencies. Therefore, UV/Fe^{II}NTA photolysis can be applied over a relatively broad pH range. These results also imply that UV/Fe^{II}NTA system has a different mechanism with UV/NTA system, by which the effect of proton is minimized.

3.4.3 Fe^{II}:NTA molar ratios and Fe^{II}NTA concentrations

The effect of Fe^{II}:NTA molar ratio was investigated by fixing the concentration of NTA at 2 mM and changing the Fe^{II} concentration from 0.1 mM to 1.0 mM. The time profiles of PFOS degradation and defluorination at different Fe^{II}:NTA molar ratios are illustrated in **Fig. S12B** in the **SI**. In general, the addition of Fe^{II} over the range of 0.1-1.0 mM enhanced PFOS degradation and defluorination compared with the UV/NTA system, except that 1.0 mM Fe^{II} resulted in a slight inhibition of PFOS degradation. However, the highest PFOS degradation and defluorination efficiencies were obtained with the Fe^{II}:NTA ratio of 0.3/2.0. This is because as the reaction proceeded, the chelating ligand was also consumed. When the chelator was in excess over Fe^{II}, the free chelator could recapture the metal ions released from the destroyed L-Fe chelate, avoid iron precipitation and guarantee the photoreductive reaction proceed continuously. In addition, NTA can also effectively reduce Fe^{III} back to Fe^{II} under UV irradiation [69], thus accelerating the Fe^{III}/Fe^{II} redox cycle. Therefore, excess NTA which serves as the sacrificial electron donor, is needed for continuous PFOS defluorination. The optimal

Fe^{II}:NTA ratio in the present study was 0.3/2.0.

In addition, the effect of Fe^{II}NTA concentration was investigated. As is shown in **Fig. S12C** in the **SI**, a doubling of [Fe^{II}NTA] accelerated PFOS degradation and defluorination, but the relative enhancement was not as significant as observed in the UV/NTA/PFOS system [21], especially during the initial stages of photolysis. This is because during the early stage of photolysis, [Fe^{II}NTA] was in excess of [PFOS], thus limiting the capacity of Fe^{II}NTA to bind PFOS. This result is consistent with the proposed mechanism that the photoinduced intramolecular electron transfer is the rate limiting step leading to PFOS degradation in this UV/Fe^{II}NTA system instead of production of e_{aq}^-.

4. Conclusions and Implications

As a potent nucleophile, e_{aq}^- has been shown to be effective in the photolytic reductive decomposition of recalcitrant organic pollutants such as PFOS. However, due to competitive back and side reactions, the e_{aq}^- can react with any electron acceptor. In order to increase the steady-state concentration of e_{aq}^-, high energy inputs or extreme conditions are required. They include raising reaction temperature [25], applying high photon fluxes [23] and the need for alkaline conditions [21]. The UV/Fe^{II}NTA system, developed as a novel photoreductive process for PFOS degradation, extends the pH range for application from the usual highly alkaline conditions down toward circumneutral pH. Meanwhile, by the coordination of Fe^{II}, a linkage is constructed between the electron donor and acceptor, which allows the occurrence of a photoinduced intramolecular charge transfer and thereby increases the electron

selectivity. Compared with the e_{aq}^- photoreduction process, photoinduced intramolecular charge transfer process has a lower activation energy, a wider pH range for application and a higher electron transfer efficiency. A comparison between UV/Fe^{II}NTA and UV/NTA system is shown in **Table S5, SI**. Considering that the photocatalytic activity of metal-ligand complexes depends on the specific metal ion employed and the donating capability of the coordinating ligands, designing more efficient chelates as the photocatalyst is desirable.

Mixed redox state metal-ligand complexes such as the Fe^{II}/Fe^{III}-APCAs have been widely used in photo-Fenton and electro-Fenton systems to activate H_2O_2 or persulfate in various advanced oxidation processes (AOPs). The present study indicates that Fe^{II}/Fe^{III}-APCAs can also be used to catalyze the photoreduction of PFOS in the absence of oxygen. Therefore, combined or sequential reactors can be further employed in a treatment train process [75], in which the reduction or oxidation can be easily operated by controlling the gas-phase atmosphere and by adding specific reductants or oxidants. In such cases, the reductive and oxidative processes are employed synergistically for targeted pollution control, for example, of PFAS, in order to effect total mineralization.

Acknowledgements

The authors are thankful for the contributions of Prof. Le Wang of the College of Materials Science and Engineering at Donghua University and Prof. Guangfeng Wei of the School of Chemical Science and Engineering at Tongji University for their assistance with DFT calculations and for improving our discussion of results. This study

was supported by the National Natural Science Foundation of China (Grant No. 21906016, 21976135, 21677109), the Fundamental Research Funds for the Central Universities (Grant No. 2232020D-25) and the State Key Laboratory of Pollution Control and Resource Reuse Foundation (Grant No. PCRRF19007).

References

[1] R. Renner, Growing concern over perfluorinated chemicals, Environmental science & technology 35(7) (2001) 154A-160A.

[2] J.P. Giesy, K. Kannan, Peer reviewed: perfluorochemical surfactants in the environment, Environmental science & technology 36(7) (2002) 146A-152A.

[3] KEMI (Swedish Chemicals Agency), Occurrence and use of highly fluorinated substances and alternatives, (2015). http://www.kemi.se/en/global/rapporter/2015/report-7-15-occurrence-and-use-of-highlyfluorinated-substances-and-alternatives.pdf.

[4] Z.Y. Wang, J.C. DeWitt, C.P. Higgins, I.T. Cousins, A Never-Ending Story of Per- and Polyfluoroalkyl Substances (PFASs)?, Environmental Science & Technology 51(5) (2017) 2508-2518. https://doi.org/10.1021/acs.est.6b04806.

[5] C. Lau, K. Anitole, C. Hodes, D. Lai, A. Pfahles-Hutchens, J. Seed, Perfluoroalkyl acids: A review of monitoring and toxicological findings, Toxicological Sciences 99(2) (2007) 366-394. https://doi.org/10.1093/toxsci/kfm128.

[6] K. Prevedouros, I.T. Cousins, R.C. Buck, S.H. Korzeniowski, Sources, fate and transport of perfluorocarboxylates, Environmental Science & Technology 40(1) (2006) 32-44. https://doi.org/10.1021/es0512475.

[7] A.G. Paul, K.C. Jones, A.J. Sweetman, A First Global Production, Emission, And Environmental Inventory For Perfluorooctane Sulfonate, Environmental Science & Technology 43(2) (2009) 386-392. https://doi.org/10.1021/es802216n.

[8] S. Kim, I. Thapar, B.W. Brooks, Epigenetic changes by per- and polyfluoroalkyl substances (PFAS), Environmental Pollution 279 (2021) 13. https://doi.org/10.1016/j.envpol.2021.116929.

[9] P. Tarapore, B. Ouyang, Perfluoroalkyl Chemicals and Male Reproductive Health: Do PFOA and PFOS Increase Risk for Male Infertility?, Int. J. Environ. Res. Public Health 18(7) (2021) 20. https://doi.org/10.3390/ijerph18073794.

[10] H. Park, C.D. Vecitis, J. Cheng, N.F. Dalleska, B.T. Mader, M.R. Hoffmann, Reductive degradation of perfluoroalkyl compounds with aquated electrons generated from iodide photolysis at 254 nm, Photochemical & Photobiological Sciences 10(12) (2011) 1945-1953. https://doi.org/10.1039/c1pp05270e.

[11] S. Takagi, F. Adachi, K. Miyano, Y. Koizumi, H. Tanaka, I. Watanabe, S. Tanabe, K. Kannan, Fate of Perfluorooctanesulfonate and perfluorooctanoate in drinking water treatment processes, Water Research 45(13) (2011) 3925-3932. https://doi.org/10.1016/j.watres.2011.04.052.

[12] H. Javed, C. Lyu, R.N. Sun, D.N. Zhang, P.J.J. Alvarez, Discerning the inefficacy of hydroxyl radicals during perfluorooctanoic acid degradation, Chemosphere 247 (2020) 6. https://doi.org/10.1016/j.chemosphere.2020.125883.

[13] H. Hori, E. Hayakawa, H. Einaga, S. Kutsuna, K. Koike, T. Ibusuki, H. Kiatagawa, R. Arakawa, Decomposition of environmentally persistent perfluorooctanoic acid

in water by photochemical approaches, Environmental Science & Technology 38(22) (2004) 6118-6124. https://doi.org/10.1021/es049719n.

[14] H. Moriwaki, Y. Takagi, M. Tanaka, K. Tsuruho, K. Okitsu, Y. Maeda, Sonochemical decomposition of perfluorooctane sulfonate and perfluorooctanoic acid, Environmental Science & Technology 39(9) (2005) 3388-3392. https://doi.org/10.1021/es040342v.

[15] H. Hori, Y. Nagaoka, A. Yamamoto, T. Sano, N. Yamashita, S. Taniyasu, S. Kutsuna, I. Osaka, R. Arakawa, Efficient decomposition of environmentally persistent perfluorooctanesulfonate and related fluorochemicals using zerovalent iron in subcritical water, Environmental science & technology 40(3) (2006) 1049-1054.

[16] J.E. Zenobio, M. Modiri-Gharehveran, C. de Perre, C.D. Vecitis, L.S. Lee, Reductive transformation of perfluorooctanesulfonate by nNiFe(0)-Activated carbon, J. Hazard. Mater. 397 (2020) 10. https://doi.org/10.1016/j.jhazmat.2020.122782.

[17] Y.C. Lee, S.L. Lo, P.T. Chiueh, D.G. Chang, Efficient decomposition of perfluorocarboxylic acids in aqueous solution using microwave-induced persulfate, Water Research 43(11) (2009) 2811-2816. https://doi.org/10.1016/j.watres.2009.03.052.

[18] C.E. Schaefer, C. Andaya, A. Burant, C.W. Condee, A. Urtiaga, T.J. Strathmann, C.P. Higgins, Electrochemical treatment of perfluorooctanoic acid and perfluorooctane sulfonate: Insights into mechanisms and application to

groundwater treatment, Chem. Eng. J. 317 (2017) 424-432. https://doi.org/10.1016/j.cej.2017.02.107.

[19] K. Yasuoka, K. Sasaki, R. Hayashi, An energy-efficient process for decomposing perfluorooctanoic and perfluorooctane sulfonic acids using dc plasmas generated within gas bubbles, Plasma Sources Sci. Technol. 20(3) (2011) 7. https://doi.org/10.1088/0963-0252/20/3/034009.

[20] G.V. Buxton, C.L. Greenstock, W.P. Helman, A.B. Ross, Critical review of rate constants for reactions of hydrated electrons, hydrogen atoms and hydroxyl radicals (· OH/· O− in aqueous solution, Journal of physical and chemical reference data 17(2) (1988) 513-886.

[21] Z. Sun, C. Zhang, L. Xing, Q. Zhou, W. Dong, M.R. Hoffmann, UV/Nitrilotriacetic Acid Process as a Novel Strategy for Efficient Photoreductive Degradation of Perfluorooctanesulfonate, Environmental science & technology 52(5) (2018) 2953-2962. https://doi.org/10.1021/acs.est.7b05912.

[22] Y. Qu, C.J. Zhang, P. Chen, Q. Zhou, W.X. Zhang, Effect of initial solution pH on photo-induced reductive decomposition of perfluorooctanoic acid, Chemosphere 107 (2014) 218-223. https://doi.org/10.1016/j.chemosphere.2013.12.046.

[23] Y.R. Gu, W.Y. Dong, C. Luo, T.Z. Liu, Efficient Reductive Decomposition of Perfluorooctanesulfonate in a High Photon Flux UV/Sulfite System, Environmental Science & Technology 50(19) (2016) 10554-10561. https://doi.org/10.1021/acs.est.6b03261.

[24] J. Gu, L. Yang, J. Ma, J. Jiang, J.X. Yang, J.Q. Zhang, H.Z. Chi, Y. Song, S.F. Sun,

W.Q. Tian, Hydrated electron (e(aq)(-)) generation from p-benzoquinone/UV: Combined experimental and theoretical study, Appl. Catal. B-Environ. 212 (2017) 150-158. https://doi.org/10.1016/j.apcatb.2017.03.081.

[25] X.J. Lyu, W.W. Li, P.K.S. Lam, H.Q. Yu, Insights into perfluorooctane sulfonate photodegradation in a catalyst-free aqueous solution, Sci Rep 5 (2015) 6. https://doi.org/10.1038/srep09353.

[26] I. Bauer, H.J. Knolker, Iron Catalysis in Organic Synthesis, Chemical Reviews 115(9) (2015) 3170-3387. https://doi.org/10.1021/cr500425u.

[27] J.R. McKone, S.C. Marinescu, B.S. Brunschwig, J.R. Winkler, H.B. Gray, Earth-abundant hydrogen evolution electrocatalysts, Chem. Sci. 5(3) (2014) 865-878. https://doi.org/10.1039/c3sc51711j.

[28] J.J. Soldevila-Barreda, N. Metzler-Nolte, Intracellular Catalysis with Selected Metal Complexes and Metallic Nanoparticles: Advances toward the Development of Catalytic Metallodrugs, Chemical Reviews 119(2) (2019) 829-869. https://doi.org/10.1021/acs.chemrev.8b00493.

[29] R.S. Shukla, A. Robert, B. Meunier, Kinetic investigations of oxidative degradation of aromatic pollutant 2,4,6-trichlorophenol by an iron-porphyrin complex, a model of ligninase, J. Mol. Catal. A-Chem. 113(1-2) (1996) 45-49. https://doi.org/10.1016/s1381-1169(96)00105-7.

[30] L. Jin, P.Y. Zhang, T. Shao, S.L. Zhao, Ferric ion mediated photodecomposition of aqueous perfluorooctane sulfonate (PFOS) under UV irradiation and its mechanism, J. Hazard. Mater. 271 (2014) 9-15.

https://doi.org/10.1016/j.jhazmat.2014.01.061.

[31] Y. Wang, P.Y. Zhang, G. Pan, H. Chen, Ferric ion mediated photochemical decomposition of perfluorooctanoic acid (PFOA) by 254 nm UV light, J. Hazard. Mater. 160(1) (2008) 181-186. https://doi.org/10.1016/j.jhazmat.2008.02.105.

[32] Y.J. Yuan, L.Z. Feng, N. Xie, L.Z. Zhang, J.M. Gong, Rapid photochemical decomposition of perfluorooctanoic acid mediated by a comprehensive effect of nitrogen dioxide radicals and Fe3(+/)Fe(2+) redox cycle, J. Hazard. Mater. 388 (2020) 9. https://doi.org/10.1016/j.jhazmat.2019.121730.

[33] J.H. Cheng, X.Y. Liang, S.W. Yang, Y.Y. Hu, Photochemical defluorination of aqueous perfluorooctanoic acid (PFOA) by VUV/Fe3+ system, Chem. Eng. J. 239 (2014) 242-249. https://doi.org/10.1016/j.cej.2013.11.023.

[34] L. Jin, P.Y. Zhang, T. Shao, Factors Influencing the Ferric Ion-mediated Photochemical Decomposition of Perfluorooctane Sulfonate (PFOS) in Water, J. Adv. Oxid. Technol. 18(1) (2015) 147-154.

[35] S.A. Messele, C. Bengoa, F.E. Stuber, J. Giralt, A. Fortuny, A. Fabregat, J. Font, Enhanced Degradation of Phenol by a Fenton-Like System (Fe/EDTA/H2O2) at Circumneutral pH, Catalysts 9(5) (2019) 14. https://doi.org/10.3390/catal9050474.

[36] Y. Wang, P.Y. Zhang, Enhanced photochemical decomposition of environmentally persistent perfluorooctanoate by coexisting ferric ion and oxalate, Environmental Science and Pollution Research 23(10) (2016) 9660-9668. https://doi.org/10.1007/s11356-016-6205-4.

[37] Y. Wang, X.Y. Shi, Photochemical Degradation of Perfluorocarboxylic Acids

Induced by Ferric Ion: Effects of pH and Carbon Chain, Acta Chim. Sin. 72(6) (2014) 682-688. https://doi.org/10.6023/a14020101.

[38] E. Repo, J.K. Warchol, A. Bhatnagar, A. Mudhoo, M. Sillanpaa, Aminopolycarboxylic acid functionalized adsorbents for heavy metals removal from water, Water Research 47(14) (2013) 4812-4832. https://doi.org/10.1016/j.watres.2013.06.020.

[39] J. De Laat, Y.H. Dao, N.H. El Najjar, C. Daou, Effect of some parameters on the rate of the catalysed decomposition of hydrogen peroxide by iron(III)-nitrilotriacetate in water, Water Research 45(17) (2011) 5654-5664. https://doi.org/10.1016/j.watres.2011.08.028.

[40] R.J. Motekaitis, A.E. Martell, The iron(III) and iron(II) complexes of nitrilotriacetic acid, Journal of Coordination Chemistry 31(1) (1994) 67-78. https://doi.org/10.1080/00958979408022546.

[41] S. Bashir, M. Mustafa, S.W. Safvi, N.A. Farhad, M.A. Rizvi, Iron Reduces Iron: A Spectroelectrochemical Insight of Ligand Effect on Iron Redox Potential, Chiang Mai J. Sci. 45(2) (2018) 1087-1098.

[42] Z. Wang, W. Qiu, S.Y. Pang, J. Jiang, Effect of chelators on the production and nature of the reactive intermediates formed in Fe(II) activated peroxydisulfate and hydrogen peroxide processes, Water Research 164 (2019) 9. https://doi.org/10.1016/j.watres.2019.114957.

[43] Y. Wang, X. Yuan, X.M. Li, F.B. Li, T.X. Liu, Ligand mediated reduction of c-type cytochromes by Fe(II): Kinetic and mechanistic insights, Chem. Geol. 513 (2019)

23-31. https://doi.org/10.1016/j.chemgeo.2019.03.006.

[44] Y.Q. Zhang, Q.Z. Zhang, S.J. Zuo, M.H. Zhou, Y.W. Pan, G.B. Ren, Y.C. Li, Y. Zhang, A highly efficient flow-through electro-Fenton system enhanced with nitrilotriacetic acid for phenol removal at neutral pH, Science of the Total Environment 697 (2019) 8. https://doi.org/10.1016/j.scitotenv.2019.134173.

[45] J. Lati, D. Meyerstein, Oxidation of first-row bivalent transition-metal complexes containing ethylenediaminetetraacetate and nitrilotriacetate ligands by free radicals. A pulse-radiolysis study, ChemInform 9(51) (1978).

[46] K. Sahul, B.K. Sharma, Gamma radiolysis of nitrilotriacetic acid (nta) in aqueous solutions, J. Radioanal. Nucl. Chem. 109(2) (1987) 321-327.

[47] R.O. Rahn, Potassium iodide as a chemical actinometer for 254 nm radiation: use of iodate as an electron scavenger, Photochemistry and Photobiology 66(6) (1997) 885-885.

[48] J.Y. Jin, S.J. Zhang, B.D. Wu, Z.H. Chen, G.Y. Zhang, P.G. Tratnyek, Enhanced Photooxidation of Hydroquinone by Acetylacetone, a Novel Photosensitizer and Electron Shuttle, Environmental Science & Technology 53(19) (2019) 11232-11239. https://doi.org/10.1021/acs.est.9b02751.

[49] J.L. Calais, Density-functional theory of atoms and molecules. R.G. Parr and W. Yang, Oxford University Press, New York, Oxford, 1989. IX + 333 pp. Price 45.00, International Journal of Quantum Chemistry 47(1) (1993) 431-9.

[50] K. Burke, Perspective on density functional theory, J. Chem. Phys. 136(15) (2012) 9. https://doi.org/10.1063/1.4704546.

[51] Ditchfield, R., Self-Consistent Molecular-Orbital Methods. IX. An Extended Gaussian-Type Basis for Molecular-Orbital Studies of Organic Molecules, J. Chem. Phys. 54(2) (1971) 724-728.

[52] Francl, M. Michelle, Self-consistent molecular orbital methods. XXIII. A polarization-type basis set for second-row elements, J.chem.physics 77(7) (1982) 3654-3665.

[53] M.S. Gordon, J.S. Binkley, J.A. Pople, W.J. Pietro, W.J. Hehre, Self-consistent molecular-orbital methods. 22. Small split-valence basis sets for second-row elements, J. Am. Chem. Soc. 104 (1982) 2797-2803. https://doi.org/10.1021/ja00374a017.

[54] P.C.P. Hariharan, J.A. Pople, The influence of polarization functions on molecular orbital hydrogenation energies, Theoretica chimica acta 28 (1973) 213-222.

[55] Hehre, J. W., Self—Consistent Molecular Orbital Methods. XII. Further Extensions of Gaussian—Type Basis Sets for Use in Molecular Orbital Studies of Organic Molecules, J. Chem. Phys. 56(5) (1972) 2257-2261.

[56] V.A. Rassolov, J.A. Pople, M.A. Ratner, T.L. Windus, 6-31G* basis set for atoms K through Zn, J. Chem. Phys. 109(4) (1998) 1223-1229.

[57] S. Grimme, S. Ehrlich, L. Goerigk, Effect of the Damping Function in Dispersion Corrected Density Functional Theory, J. Comput. Chem. 32(7) (2011) 1456-1465. https://doi.org/10.1002/jcc.21759.

[58] M.J. Frisch, G.W. Trucks, H.B. Schlegel, G.E. Scuseria, M.A. Robb, J.R. Cheeseman, G. Scalmani, V. Barone, G.A. Petersson, H. Nakatsuji, X. Li, M.

Caricato, A.V. Marenich, J. Bloino, B.G. Janesko, R. Gomperts, B. Mennucci, H.P. Hratchian, J.V. Ortiz, A.F. Izmaylov, J.L. Sonnenberg, D. Williams-Young, F. Ding, F. Lipparini, F. Egidi, J. Goings, B. Peng, A. Petrone, T. Henderson, D. Ranasinghe, V.G. Zakrzewski, J. Gao, N. Rega, G. Zheng, W. Liang, M. Hada, M. Ehara, K. Toyota, R. Fukuda, J. Hasegawa, M. Ishida, T. Nakajima, Y. Honda, O. Kitao, H. Nakai, T. Vreven, K. Throssell, J.A. Montgomery, Jr., J.E. Peralta, F. Ogliaro, M.J. Bearpark, J.J. Heyd, E.N. Brothers, K.N. Kudin, V.N. Staroverov, T.A. Keith, R. Kobayashi, J. Normand, K. Raghavachari, A.P. Rendell, J.C. Burant, S.S. Iyengar, J. Tomasi, M. Cossi, J.M. Millam, M. Klene, C. Adamo, R. Cammi, J.W. Ochterski, R.L. Martin, K. Morokuma, O. Farkas, J.B. Foresman, D.J. Fox, Gaussian 16, Revision B.01, Gaussian, Inc., Wallingford CT, 2016.

[59] T. Yanai, D.P. Tew, N.C. Handy, A new hybrid exchange-correlation functional using the Coulomb-attenuating method (CAM-B3LYP), Chem. Phys. Lett. 393(1-3) (2004) 51-57. https://doi.org/10.1016/j.cplett.2004.06.011.

[60] R. Krishnan, J.S. Binkley, R. Seeger, J.A. Pople, Self-consistent molecular orbital methods. XX. A basis set for correlated wave functions, J. Chem. Phys. 72 (1980) 650-654. https://doi.org/10.1063/1.438955.

[61] S. Grimme, J. Antony, S. Ehrlich, H. Krieg, A consistent and accurate ab initio parametrization of density functional dispersion correction (DFT-D) for the 94 elements H-Pu, J. Chem. Phys. 132(15) (2010) 19. https://doi.org/10.1063/1.3382344.

[62] Y. Zhao, D.G. Truhlar, The M06 suite of density functionals for main group

thermochemistry, thermochemical kinetics, noncovalent interactions, excited states, and transition elements: two new functionals and systematic testing of four M06-class functionals and 12 other functionals, Theor. Chem. Acc. 120(1-3) (2008) 215-241. https://doi.org/10.1007/s00214-007-0310-x.

[63] T. Lu, F. Chen, Multiwfn: A multifunctional wavefunction analyzer, J. Comput. Chem. (2012).

[64] D.K. Schulten, VMD: Visual molecular dynamics, Journal of Molecular Graphics (1996).

[65] T. Yamamoto, Y. Noma, S.-I. Sakai, Y. Shibata, Photodegradation of perfluorooctane sulfonate by UV irradiation in water and alkaline 2-propanol, Environmental Science & Technology 41(16) (2007) 5660-5665. https://doi.org/10.1021/es0706504.

[66] H. Hori, A. Yamamoto, K. Koike, S. Kutsuna, I. Osaka, R. Arakawa, Photochemical decomposition of environmentally persistent short-chain perfluorocarboxylic acids in water mediated by iron(II)/(III) redox reactions, Chemosphere 68(3) (2007) 572-578. https://doi.org/10.1016/j.chemosphere.2006.12.038.

[67] M. Ohno, M. Ito, R. Ohkura, R.M.A. Esteban, T. Kose, T. Okuda, S. Nakai, K. Kawata, W. Nishijima, Photochemical decomposition of perfluorooctanoic acid mediated by iron in strongly acidic conditions, J. Hazard. Mater. 268 (2014) 150-155. https://doi.org/10.1016/j.jhazmat.2013.12.059.

[68] W.B. Fortune, M.G. Mellon, Determination of iron with o-phenanthroline - A

spectrophotometric study, 10 ed., Ind. Eng. Chem., Anal.1938.

[69] S.L. Andrianirinaharivelo, J.F. Pilichowski, M. Bolte, Nitrilotriacetic acid transformation photoinduced by complexation with iron(III) in aqueous-solution, Transit. Met. Chem. 18(1) (1993) 37-41. https://doi.org/10.1007/bf00136046.

[70] H. Abramczyk, J. Kroh, Absorption spectrum of the solvated electron. 2. Numerical calculations of the profiles of the electron in water and methanol at 300 K, The Journal of Physical Chemistry 95(16) (1991) 6155-6159.

[71] E.J. Hart, J. Boag, Absorption spectrum of the hydrated electron in water and in aqueous solutions, Journal of the American Chemical Society 84(21) (1962) 4090-4095.

[72] Y. Bao, Theoretical study on the structural and electronic properties and the decomposition mechanism of PFOS, Inner Mongolia Normal University, Inner Mongolia Normal University, 2013.

[73] C. Zhang, Y. Qu, X. Zhao, Q. Zhou, Photoinduced Reductive Decomposition of Perflurooctanoic Acid in Water: Effect of Temperature and Ionic Strength, Clean-Soil Air Water 43(2) (2015) 223-228. https://doi.org/10.1002/clen.201300869.

[74] P.J. Krusic, D.C. Roe, Gas-phase NMR technique for studying the thermolysis of materials: Thermal decomposition of ammonium perfluorooctanoate, Anal. Chem. 76(13) (2004) 3800-3803. https://doi.org/10.1021/ac049667k.

[75] D.N. Lu, S. Sha, J.Y. Luo, Z.R. Huang, X.Z. Jackie, Treatment train approaches for the remediation of per- and polyfluoroalkyl substances (PFAS): A critical review, J. Hazard. Mater. 386 (2020) 14.

https://doi.org/10.1016/j.jhazmat.2019.121963.

Figure Captions

Fig. 1. The time profiles of PFOS degradation (a) and defluorination (b) under different conditions. The treatment experiment: PFOS (0.01 mM), Fe^{II}NTA (Fe^{II}: 0.3 mM; NTA: 2 mM), UV irradiation, N_2 saturated, pH (8.0); the 1st control experiment: PFOS (0.01 mM), NTA (2 mM); UV irradiation, N_2 saturated, pH (8.0); the 2nd control experiment: PFOS (0.01 mM), Fe^{2+} (0.3 mM), UV irradiation, N_2 saturated, pH (8.0); the 3rd control experiment: PFOS (0.01 mM), UV irradiation, N_2 saturated, pH (8.0). Error bars represent standard deviations of triplicate assays.

Fig. 2. (a) Transient absorption spectra following the laser flash photolysis of 1.5 mM Fe^{II} complexed with 10 mM NTA at pH 8.0. (b) Decay of e_{aq}^- detected at 700 nm in Fe^{II}NTA system in the presence of PFOS with different concentrations. The transient absorption curves were also fitted. (c) Transient absorption curve recorded at 700 nm under different conditions. The concentrations of the metal ions and NTA were 1.5 mM and 10 mM, respectively. The initial pH of the metal-NTA solutions were all adjusted to 8.0. (d) The partially enlarged view of (c).

Fig. 3. TDDFT simulated spectrum of the pentacoordinated [PFOS-Fe^{II}-NTA] complex and the electron transitions in the excited states, which are listed in Table S3. Isosurface plots of the frontier MOs computed at 0.05 au.

Fig. 4. The time profiles of PFOS degradation (a) and defluorination (b) in the presence of various model chelates: metal ions (Fe^{2+}, Fe^{3+}, Co^{2+} or Cu^{2+}: 0.3 mM), model ligands (NTA, DTPA, IDA, CA or MGDA: 2 mM), PFOS (0.01 mM), UV irradiation, N_2 saturated, pH (8.0).

Declaration of interests

☒ The authors declare that they have no known competing financial interests or personal relationships that could have appeared to influence the work reported in this paper.

☐The authors declare the following financial interests/personal relationships which may be considered as potential competing interests:

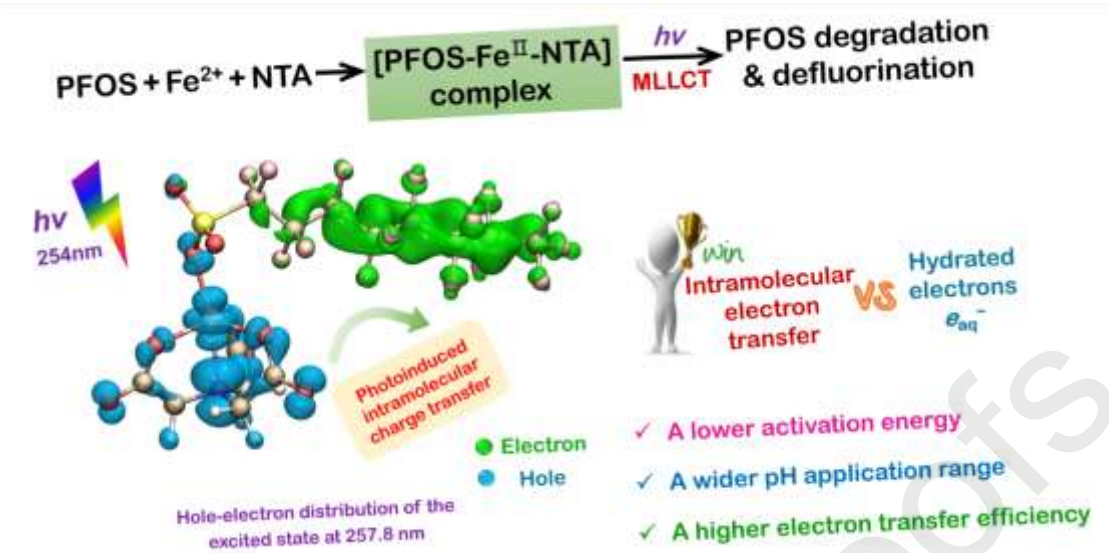

Highlights

UV/Fe^{II}NTA system decomposes PFOS effectively under circumneutral conditions.

A concerted photoinduced intramolecular charge transfer mechanism is involved.

The properties of metal ions and ligands determine the photocatalytic efficiency.

A higher electron transfer efficiency is obtained than e_{aq}^- reduction.

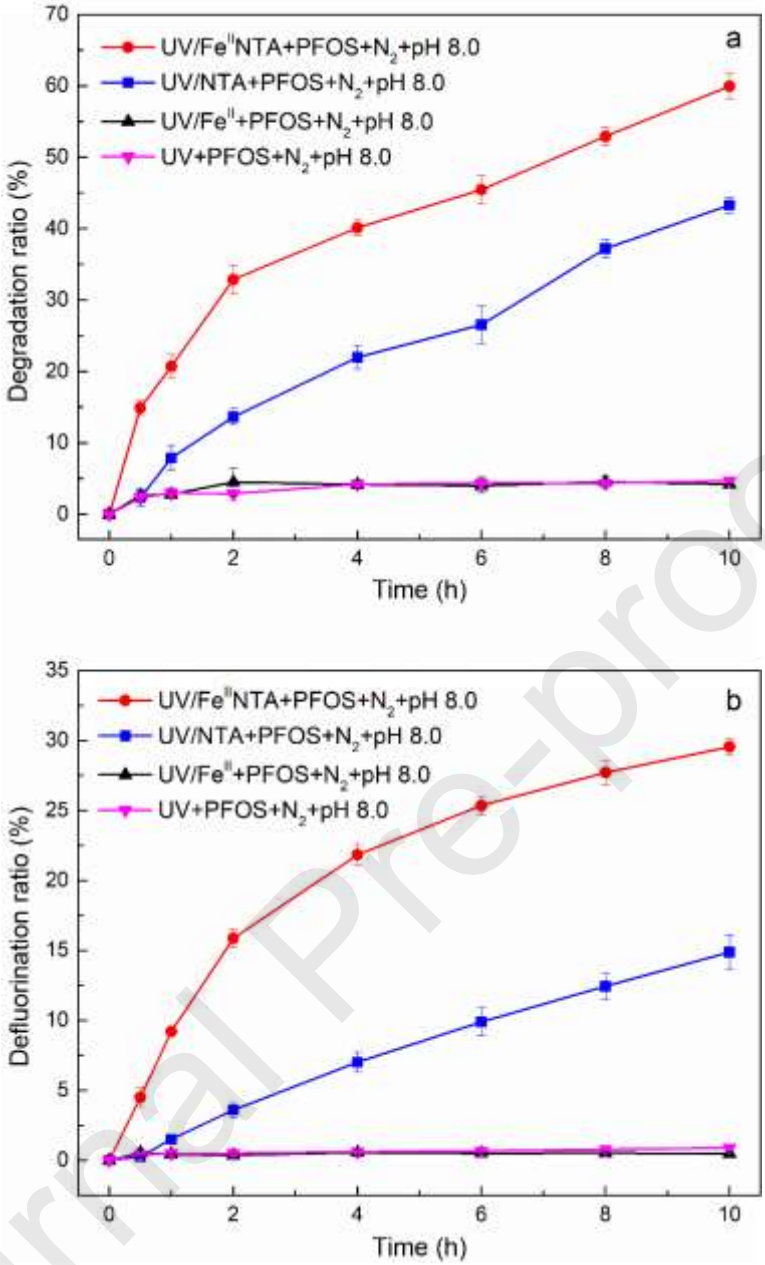

Fig. 1. The time profiles of PFOS degradation (a) and defluorination (b) under different conditions. The treatment experiment: PFOS (0.01 mM), $Fe^{II}NTA$ (Fe^{II}: 0.3 mM; NTA: 2 mM), UV irradiation, N_2 saturated, pH (8.0); the 1st control experiment: PFOS (0.01 mM), NTA (2 mM); UV irradiation, N_2 saturated, pH (8.0); the 2nd control experiment: PFOS (0.01 mM), Fe^{2+} (0.3 mM), UV irradiation, N_2 saturated, pH (8.0); the 3rd control experiment: PFOS (0.01 mM), UV irradiation, N_2 saturated, pH (8.0). Error bars represent standard deviations of triplicate assays.

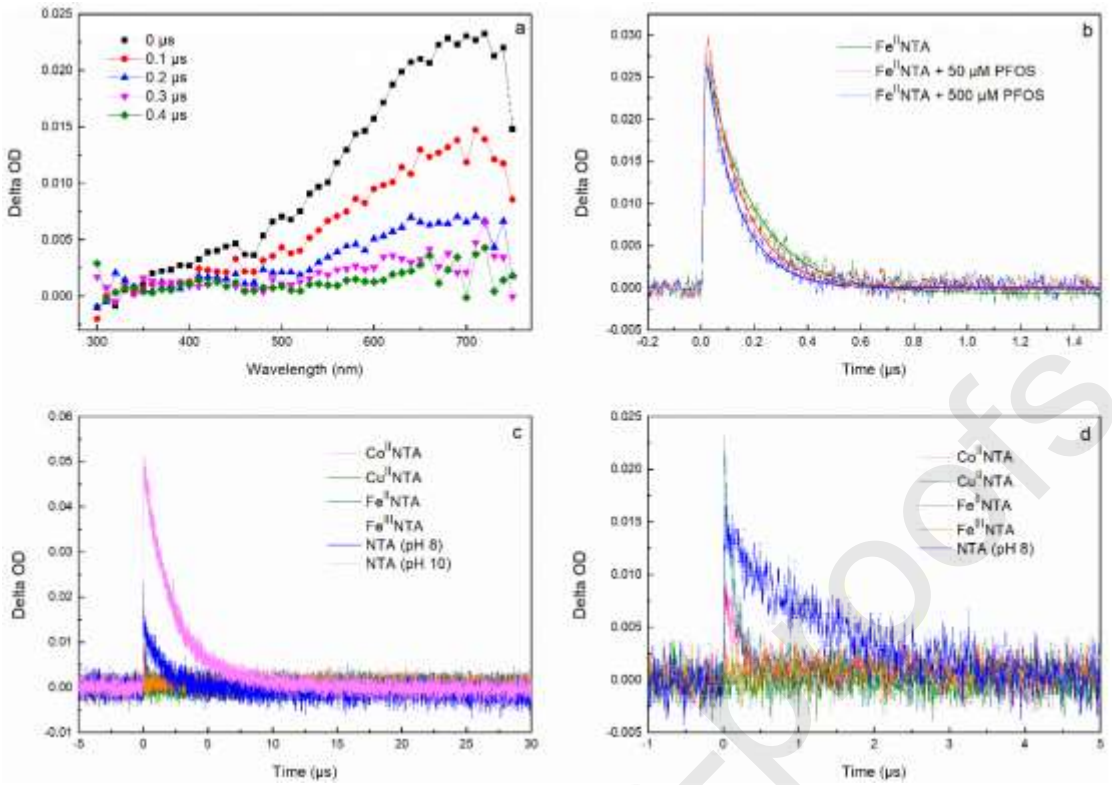

Fig. 2. (a) Transient absorption spectra following the laser flash photolysis of 1.5 mM Fe^{II} complexed with 10 mM NTA at pH 8.0. (b) Decay of e_{aq}^- detected at 700 nm in Fe^{II}NTA system in the presence of PFOS with different concentrations. The transient absorption curves were also fitted. (c) Transient absorption curve recorded at 700 nm under different conditions. The concentrations of the metal ions and NTA were 1.5 mM and 10 mM, respectively. The initial pH of the metal-NTA solutions were all adjusted to 8.0. (d) The partially enlarged view of (c).

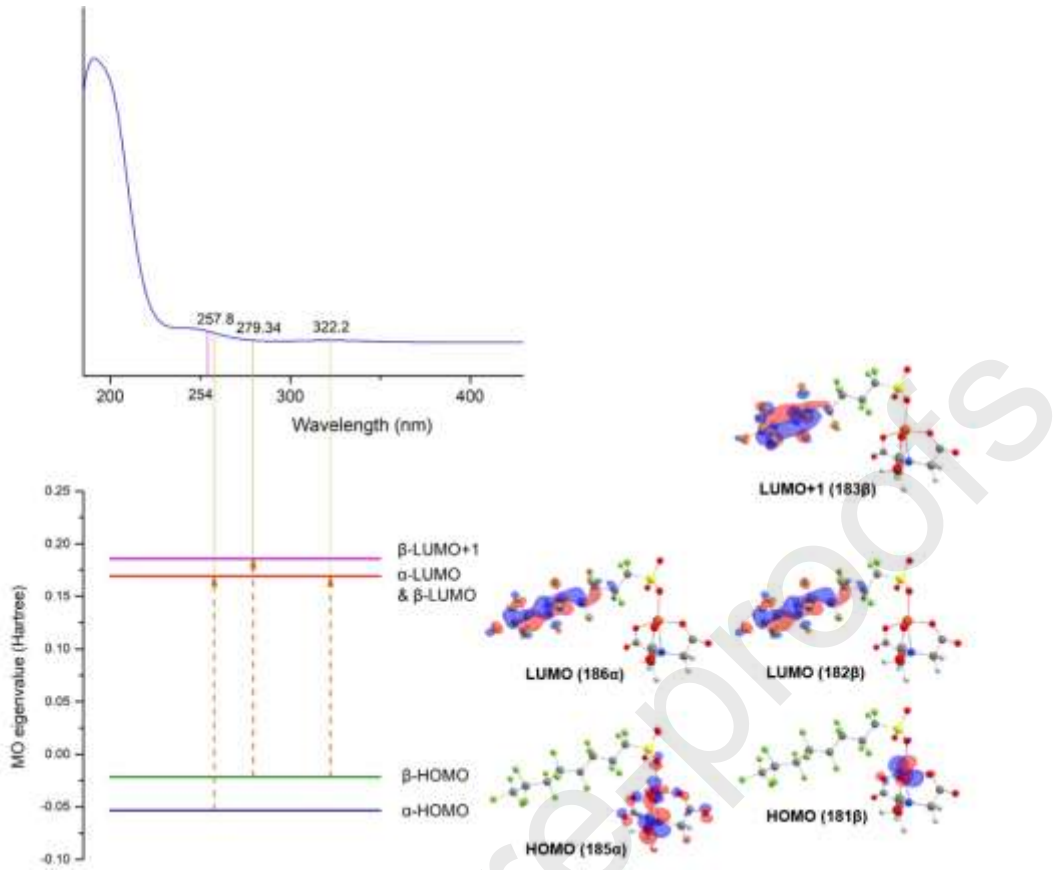

Fig. 3. TDDFT simulated spectrum of the pentacoordinated [PFOS-Fe^{II}-NTA] complex and the electron transitions in the excited states, which are listed in Table S3. Isosurface plots of the frontier MOs computed at 0.05 au.

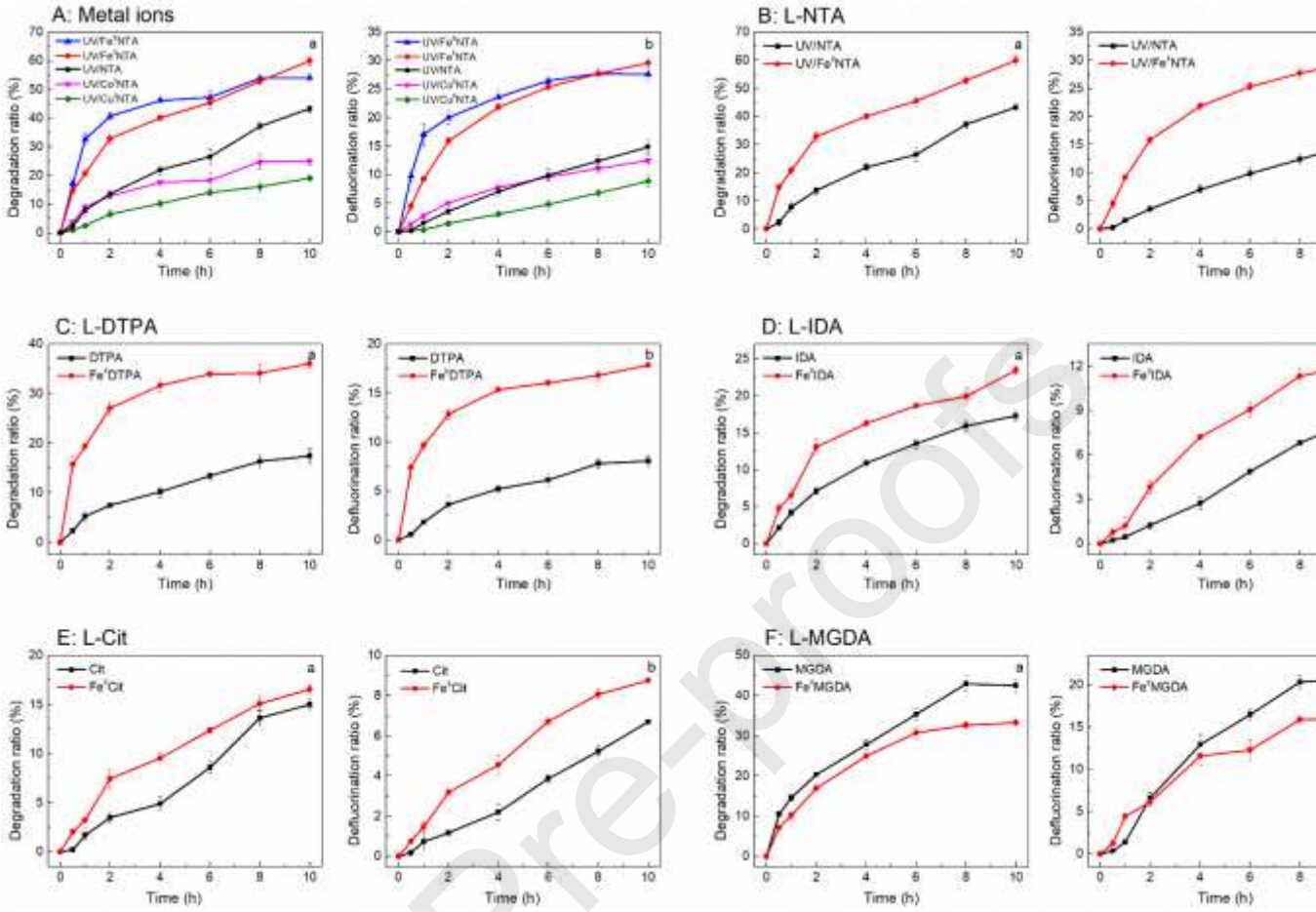

Fig. 4. The time profiles of PFOS degradation (a) and defluorination (b) in the presence of various model chelates: metal ions (Fe^{2+}, Fe^{3+}, Co^{2+} or Cu^{2+}: 0.3 mM), model ligands (NTA, DTPA, IDA, CA or MGDA: 2 mM), PFOS (0.01 mM), UV irradiation, N_2 saturated, pH (8.0).